Driven-Dissipative Time Crystalline Phases in a Two-Mode Bosonic System with Kerr Nonlinearity

L. R. Bakker,[1,2,*] M. S. Bahovadinov,[2,3] D. V. Kurlov,[2] V. Gritsev,[1,2]
A. K. Fedorov,[2,4] and Dmitry O. Krimer[5]

[1]*Institute for Theoretical Physics, Universiteit van Amsterdam, Science Park 904, Amsterdam, Netherlands*
[2]*Russian Quantum Center, Skolkovo, Moscow 143025, Russia*
[3]*Physics Department, National Research University Higher School of Economics, Moscow 101000, Russia*
[4]*National University of Science and Technology "MISIS", Moscow 119049, Russia*
[5]*Institute for Theoretical Physics, Vienna University of Technology (TU Wien), Wiedner Hauptstraße 8-10/136, A1040 Vienna, Austria*

(Received 27 May 2022; accepted 31 October 2022; published 12 December 2022)

For the driven-dissipative system of two coupled bosonic modes in a nonlinear cavity resonator, we demonstrate a sequence of phase transitions from a trivial steady state to two distinct dissipative time crystalline phases. These effects are already anticipated at the level of the semiclassical analysis of the Lindblad equation using the theory of bifurcations and are further supported by the full quantum treatment. The system is predicted to exhibit different dynamical phases characterized by an oscillating nonequilibrium steady state with nontrivial periodicity, which is a hallmark of time crystals. We expect that these phases can be directly probed in various cavity QED experiments.

DOI: 10.1103/PhysRevLett.129.250401

Introduction.—Nonlinear quantum optical effects are of great importance for fundamental research and various applications, in particular in quantum information technologies [1–6]. Realistic settings of quantum experiments require considering sizable nonlinear effects and interplay between external driving and dissipation caused by the fundamentally open nature of such systems. A system of paramount importance is a driven-dissipative model of bosonic modes with the Kerr nonlinearity [7–11]. For example, a qubit encoded in quantum harmonic oscillators [12] can be made stable against environment-induced decay using an interplay between Kerr-type interactions and squeezing [13–15]. On the fundamental side, nonequilibrium bosonic systems with Kerr nonlinearities may exhibit novel dynamical phases, such as time crystals [16–18].

Time crystal (TC) phases of matter have been predicted theoretically in isolated Floquet driven systems and driven-dissipative systems [19–31], and have recently been observed experimentally [32–37]. Time crystals were originally introduced as the temporal analogue of spatial crystals where the time translation symmetry of a system is broken [38]. Crucially, the time crystalline phase of matter would be resistant to entropy increase [32,39–41]. This property makes the TC phase an interesting candidate for quantum hardware devices, where entropy growth and spontaneous decay lead to corruption of stored information.

In this Letter we demonstrate that a system of two driven-dissipative coupled bosonic modes trapped in an optical cavity with Markovian dissipation exhibits intriguing dynamical behavior featuring *inter alia* time-crystalline phases. In the semiclassical regime, the system undergoes a series of sub- and supercritical Hopf bifurcations between different stationary solutions. Hopf bifurcations are responsible for periodic dynamics emerging in the form of limit cycles in the phase space of a system [42]–a phenomenon that is absent in a single-mode bosonic system with a Kerr nonlinearity [43,44]. Most importantly, we find period-doubling behavior suggesting the existence of multiple distinct, nontrivial TC phases in the system. The presence of limit cycles on the semiclassical level turns out to be an indicator for resulting TC phases in the full quantum dynamics, where multiple nonequilibrium phase transitions in the form of the closure of the dissipative gap in the Liouvillian spectrum are observed.

Our analytical approach is based on a combination of Lie-algebraic disentanglement techniques [45–51] and a semiclassical approximation (see Supplemental Material [52]). The results in the quantum regime are found using exact diagonalization (ED) methods and Monte Carlo simulations for trajectories of observables, which allow us to investigate larger system sizes. Using a combination of all the aforementioned methods, we conclude that different time crystalline phases exist in a broad range of values of the single-photon driving amplitude.

The model.—We consider two driven-dissipative coupled modes in a cavity [54] (see Fig. 1) described by the following Hamiltonian ($\hbar = 1$):

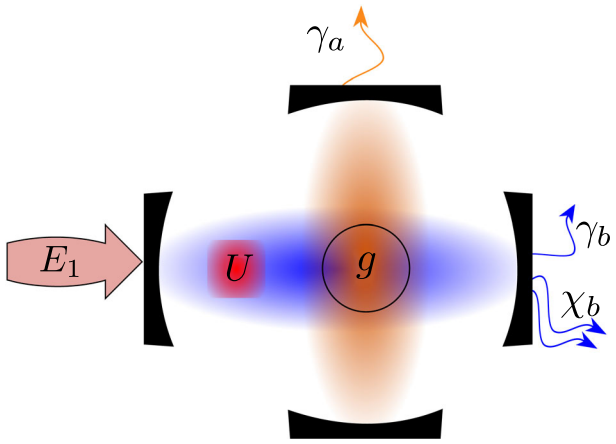

FIG. 1. Schematic representation of our setup: A cavity with two bosonic modes a (orange cloud) and b (blue cloud) coupled with a strength g to each other, see Eq. (1). A Kerr interaction with a strength U is generated by a nonlinear element (red square) for the b mode. The cavity is driven coherently by a single photon drive E_1. The cavities allow for the decay of the modes with the single-photon rates $\gamma_{a,b}$ and two-photon rate χ_b (orange and blue arrows).

$$\hat{H} = \omega_a \hat{a}^\dagger \hat{a} + g\hat{b}^\dagger \hat{a} + g^* \hat{b}\hat{a}^\dagger + \omega_b \hat{b}^\dagger \hat{b} + E_1(t)\hat{b} + E_1^*(t)\hat{b}^\dagger + \frac{U}{2}\hat{b}^\dagger \hat{b}^\dagger \hat{b}\,\hat{b}, \tag{1}$$

where $\hat{a}$, $\hat{b}$ ($\hat{a}^\dagger$, $\hat{b}^\dagger$) are bosonic annihilation (creation) operators. Parameters $\omega_j > 0$ are the cavity frequencies of the a and b modes, g is the coupling strength between the modes, $E_1(t) = \mathcal{E}_1 e^{i\omega_1 t}$ determines the driving protocol of the b mode, and U is the Kerr interaction strength. In nonlinear media $U \sim n_2\omega_0^2/(n_0^2 V_{\text{eff}})$, where $n_{0,2}$ are linear and nonlinear refractive indexes, ω_0, V_{eff} are the mode frequency and effective volume, respectively. Both a and b modes are coupled to a zero-temperature Markovian environment. The a mode experiences only single-photon losses, whereas the b mode is prone to single- and two-photon losses [55]. The overall time evolution of the system is then governed by the Lindblad equation [56],

$$\dot{\rho} = -i[\hat{H}, \rho] + \frac{\gamma_a}{2}\mathcal{D}[\hat{a}]\rho + \frac{\gamma_b}{2}\mathcal{D}[\hat{b}]\rho + \frac{\chi_b}{2}\mathcal{D}[\hat{b}^2]\rho \equiv \mathcal{L}\rho, \tag{2}$$

where $\mathcal{D}[\hat{L}]\rho = 2\hat{L}\rho\hat{L}^\dagger - \hat{L}^\dagger\hat{L}\rho - \rho\hat{L}^\dagger\hat{L}$ is the dissipator, $\hat{H}$ is given by Eq. (1), and $\mathcal{L}$ is the Liouvillian. Moreover, $\gamma_j > 0$ and $\chi_j > 0$ represent the cavity single and double mode loss rates, correspondingly.

Semiclassical analysis.—In the semiclassical approximation, the Lindblad equation is reduced to the master equation in a rotating frame with driving frequency ω_1, where the exponential term $e^{i\omega_1 t}$ vanishes [52]:

$$\dot{\boldsymbol{\xi}}(t) = \boldsymbol{A}(|z|^2)\boldsymbol{\xi}(t) + \boldsymbol{\eta}, \tag{3}$$

where

$$\boldsymbol{A}(|z|^2) = \begin{pmatrix} \tilde{\kappa}_a & -ig^* & 0 & 0 \\ -ig & \varphi(|z|^2) & 0 & 0 \\ 0 & 0 & \tilde{\kappa}_a^* & ig \\ 0 & 0 & ig^* & \varphi^*(|z|^2) \end{pmatrix}. \tag{4}$$

Here the vectors $\boldsymbol{\xi} = (y, z, y^*, z^*)^T$ and $\boldsymbol{\eta} = (0, -i\mathcal{E}_1^*, 0, i\mathcal{E}_1)^T$ are defined by $y(t) = \exp(\tilde{\kappa}_a t)\text{Tr}[\hat{a}\rho(t)]$ and $z(t) = e^{i\omega_1 t}b(t)$, $\varphi(|z|^2) = \tilde{\kappa}_b + K|z|^2$, $\tilde{\kappa}_j = -i\Delta_j - \gamma_j/2$, $\Delta_j = \omega_j - \omega_1$ for $j = a, b$, and $K = -\chi_b - iU$.

Results.—We proceed with the analysis of the semiclassical steady-state solution by setting $\dot{\boldsymbol{\xi}} = 0$ into Eq. (3) and obtain an S shape [see solid and dashed red curves in Fig. 2(a)] that is well known in systems with Kerr-type interactions [43,44,57]. Upon closer inspection, we uncover novel nontrivial system behaviors. The analysis of the dissipative system (3) is done using available tools developed for the theory of bifurcations [42,58,59]. In our system we find that the steady state solutions have several interesting features, summarized in Fig. 2(a). The steady state outside of the region of bistability (S shape) is represented by a stable stationary solution. Choosing an initial state in this interval of $\mathcal{E}_1$ and letting the system time evolve, it will relax to a stationary value on one of the (solid) red curves in Fig. 2(a). Most importantly, we find an interval of $\mathcal{E}_1$, where limit cycles are other possible time-dependent steady state solutions. In order to probe the system's behavior in more detail, we use the following approach. We start by considering a coherent drive $\mathcal{E}_1 = 0$, for which the steady state solution corresponds to zero particle number excitations in the b and a modes, as expected. As we gradually increase the value of the coherent drive [for simplicity we assume $\arg(\mathcal{E}_1) = 0$], after some transient behavior the system will settle into a respective stationary solution for the b-expectation value, which lies on the lower solid red curve starting from $z = 0$ in Fig. 2(a). In this manner we can iteratively increase the driving amplitude, following the path outlined by the magenta arrows going left to right in Fig. 2(a).

As we increase the driving amplitude to within the region of bistability, we encounter a region of instability between the points H_1 and H_2 [designated by a dashed curve in Fig. 2(a) between the aforementioned points]. The transition from stable to unstable solutions is accompanied by a subcritical Hopf bifurcation at H_1 and a supercritical Hopf bifurcation at H_2. Increasing the driving amplitude beyond H_1, the system will jump to a limit cycle solution, so that the variable z oscillates in time between some maximal and minimal values as designated by solid blue curves in this figure. The limit cycles for the driving amplitudes lying between the points PD_2 and PD_1 have qualitatively the

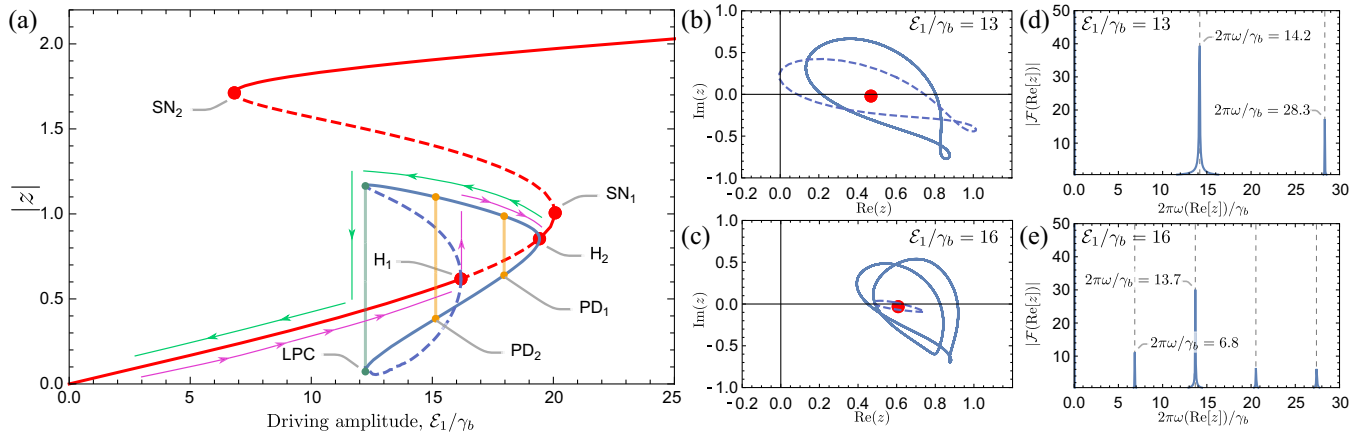

FIG. 2. (a) Solid (dashed) red curve depicts the semiclassical stable (unstable) steady state solution for the b-mode particle number, $\sqrt{n_b} = |z|$, as a function of the driving amplitude $\mathcal{E}_1$. The points H_1 and H_2 are sub- and supercritical Hopf bifurcations, respectively. Stable (unstable) limit cycles emerging from H_2 (H_1) are depicted using the solid (dashed) blue lines, indicating the absolute values in between which the oscillations occur. Stable and unstable limit cycles annihilate at the limit point cycle (LPC). $SN_{1,2}$ are saddle-node points of the optical bistability. PD_1 (PD_2) corresponds to a period-doubling bifurcation when passing this point from upper (lower) values of $\mathcal{E}_1$. Between the points PD_1 and PD_2 is the region of limit cycles with a double loop structure as shown in (c). The magenta and green arrows indicate the forward and backward sweeping paths as outlined in the main text. (b),(c) Examples of normal and period doubled limit cycles (solid blue line) and unstable limit cycle (dashed blue line) in the ($\mathrm{Re}[z]$, $\mathrm{Im}[z]$) plane. The red dot represents a stationary state lying on the lower red curve from (a). (d),(e) The Fourier spectrum of $\mathrm{Re}[z]$ of the dynamics is represented by stable limit cycles shown in (b) and (c). The system parameters are $\gamma_a = \chi_b = 1$, $g = U = \Delta_a = 10$ and $\Delta_b = -20$ (computed in units of γ_b).

same double-loop structure as exemplified in Fig. 2(c) for $\tilde{\mathcal{E}}_1/\gamma_b \approx 16$. If one keeps increasing the driving amplitude, probing the limit cycle solutions for each value of $\mathcal{E}_1$, the limit cycles will half their period at the point PD_1 in Fig. 2(a). As $\mathcal{E}_1$ increases further, their dimensions in the phase space decrease and eventually shrink to zero at the threshold point H_2, where the periodic solution ceases to exist (via the supercritical Hopf bifurcation). Above this threshold value, there is a stable stationary state between the points H_2 and SN_1.

In addition, we disclose the bifurcation scenario following an inverse route, starting from the stationary state slightly below the saddle-node bifurcation, SN_1, and gradually decreasing the driving amplitude $\mathcal{E}_1$ [green arrows going right to left in Fig. 2(a)]. This will lead to a partially different dynamical scenario associated with the hysteretic behavior shown in this figure. Specifically, when one decreases $\mathcal{E}_1$ below H_2, limit cycles are time-dependent steady states in the interval between H_2 and PD_1, as expected. Subsequently, the limit cycles double their period at PD_1. For driving amplitudes below H_1, unstable limit cycles are also possible solutions [dashed limit cycle in Fig. 2(b)] that, however, cannot be experimentally observed. At PD_2, the limit cycles half their period. With further decrease of $\mathcal{E}_1$, the stable and unstable limit cycles ultimately annihilate at the limit point cycle (LPC). When decreasing the driving amplitude below the LPC point, the time-dependent steady state will jump down to a stationary state lying on the lower red curve. Thus, on the semiclassical level, the system demonstrates a series of continuous and discontinuous phase transitions with hysteretic behavior. We note that the dynamical scenarios disclosed in this Letter are quite universal, taking place for a wide range of system parameters. A more in-depth discussion on further semiclassical scenarios and their quantum counterparts is a subject of a forthcoming publication.

In the next step, we compare the semiclassical results to the full quantum mechanical dynamics of the system. Using a representation of bosonic creation and annihilation operators in a truncated Fock basis, we compute the spectrum of our system. The thermodynamic limit is reached when the driving amplitude approaches infinity, $\mathcal{E}_1 \to \infty$, while the product $\mathcal{E}_1\sqrt{U}$ is kept fixed (the so-called "weak interaction limit") [19,60] and the product of $\mathcal{E}_1\sqrt{\chi_b}$ remains constant. We introduce a dimensionless parameter N to keep track of the particle number and quantify the large N limit as follows:

$$\mathcal{E}_1 = \tilde{\mathcal{E}}_1\sqrt{N}, \qquad U = \frac{\tilde{U}}{N}, \qquad \chi_b = \frac{\tilde{\chi}_b}{N}. \tag{5}$$

We obtain the quantum mechanical solution versus N as depicted in Fig. 3. In general, the quantum mechanical results agree to a large extent with the semiclassical predictions. In the region of optical bistability shown in Fig. 2(a) ($7 \lesssim \tilde{\mathcal{E}}_1/\gamma_b \lesssim 20$), the dissipative gap, defined as the largest real part of the nonzero eigenvalues, closes rapidly, indicating the presence of a dissipative phase transition within this region. As we increase the driving

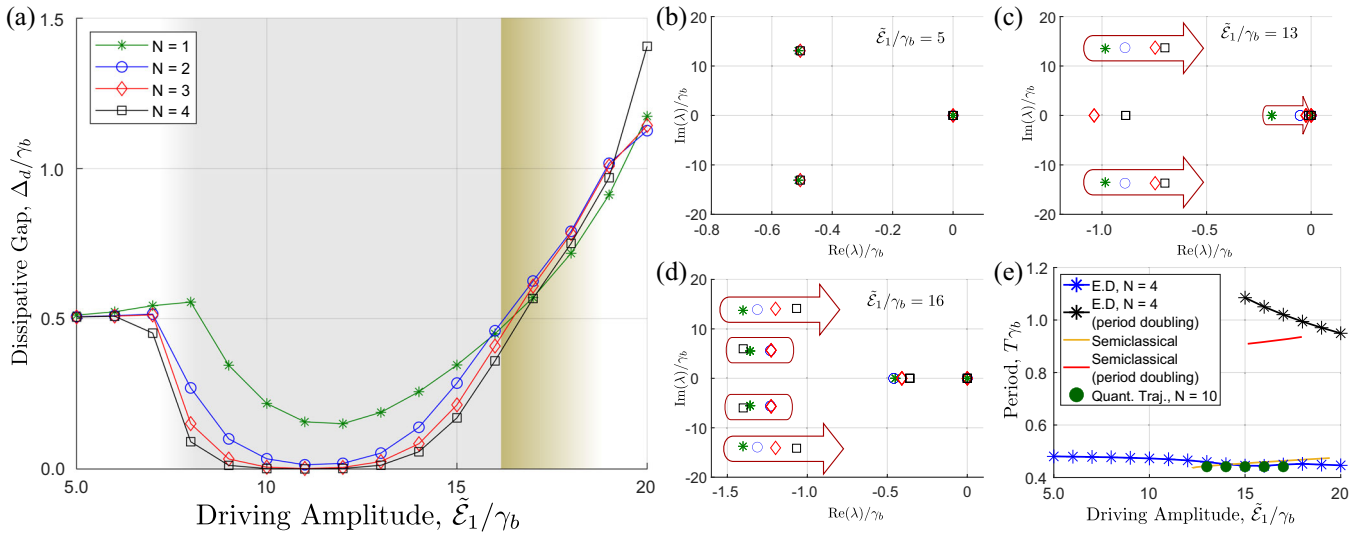

FIG. 3. (a) The dissipative gap as a function of the driving amplitude $\tilde{\mathcal{E}}_1/\gamma_b$. Qualitatively different phases are colored in by hand, based on the underlying gap closure behaviors. (b) Eigenvalues of the first few decaying modes λ_i for $\tilde{\mathcal{E}}_1/\gamma_b = 5$ and different values of N. Here, the gap does not close as we increase N. (c) The spectrum for $\tilde{\mathcal{E}}_1/\gamma_b = 13$. The arrows enclosing symbols depict how the eigenvalues converge towards the imaginary axis [$\mathrm{Re}(\lambda_i) = 0$] as a function of N. (d) Spectrum for $\tilde{\mathcal{E}}_1/\gamma_b = 16$. An additional eigenvalue enclosed in rectangles features gap closing behavior with increasing N, having an imaginary part that is about half as large as the original eigenvalues enclosed within the arrows. This eigenvalue resembles the period doubling found in the semiclassical case. (e) Periods of quantum oscillations, $T = 2\pi/\mathrm{Im}(\lambda_i)$, as a function of the driving amplitude. All system parameters are chosen the same as in Fig. 2. The results from the quantum trajectories are obtained by averaging 3000 trajectories for a duration of $t\gamma_b = 15$ with $\gamma_b dt = 0.005$ and using the software provided in [61].

amplitude to $\tilde{\mathcal{E}}_1/\gamma_b \approx 13$ (starting from $\tilde{\mathcal{E}}_1/\gamma_b \approx 7$), a pair of eigenvalues starts to approach the imaginary axis as a function of N [see Fig. 3(c)]. The resulting quantum oscillations are the quantum mechanical analogue of the limit cycles observed in the semiclassical case and indicate the time-crystalline phase. This analogy between semiclassical and quantum oscillations is derived by comparing the inverse of the imaginary parts of the eigenvalues responsible for quantum oscillations with the periods of limit cycles [see Figs. 2(d) and 2(e)]. We also note that the peaks in the Fourier spectra of Figs. 2(d) and 2(e) occur at values that scale with internal parameters of the system (e.g., $\Delta_{a,b}$, U, $\gamma_{a,b}$, etc.) in a complex way set out by a specific form of our nonlinear system (3). When increasing the driving amplitude further to a value of $\tilde{\mathcal{E}}_1/\gamma_b \approx 16$ [Fig. 3(d)], another set of eigenvalues (enclosed in ovals) starts to approach the imaginary axis with approximately half the imaginary value of the modes that were observed before (enclosed in arrows). Thus, there is a strong indication of quantum behavior resembling the period doubling found in the semiclassical case that shows up in a similar parameter range. The appearance of the modes enclosed in ovals then indicates a period doubled time crystalline phase. Unlike in the semiclassical case, however, we cannot find a signature of period *halving* in the quantum regime as we increase the driving amplitude beyond $\tilde{\mathcal{E}}_1/\gamma_b = 16$. Rather, the upper bound on the driving amplitude for the system being in the period doubled time crystal phase remains undetermined. Furthermore, in the parameter regime $\tilde{\mathcal{E}}_1/\gamma_b \gtrsim 16$ the gap closure behavior is dominated by the oscillating (hard) modes rather than the (soft) modes whose eigenvalues lie on the real axis. Evidently, a scenario in which different modes close the gap in qualitatively different ways indicates that the system experiences a series of different phase transitions. The sequence of phase transitions as a function of $\tilde{\mathcal{E}}_1/\gamma_b$ between steady state and different time crystalline phases is highlighted in Fig. 3(a) using the colored background. Different phases were identified by the relative magnitude of the gap, the eigenvalues for the modes characterizing the time crystal phase [enclosed by arrows in Figs. 3(c) and 3(d)], and the period doubled modes [enclosed by ovals in Fig. 3(d)]. At a value of $\tilde{\mathcal{E}}_1/\gamma_b \approx 16$, the time crystal mode associated with the period doubled mode is practically as dominant as the usual time crystal mode. The edges of the coloring in Fig. 3(a) are blurred, as the exact behavior of the gap for larger values of N and $\tilde{\mathcal{E}}_1$ is currently outside of computational capabilities. A full comparison of the periods of oscillatory quantum and semiclassical solutions is presented in Fig. 3(e) [52], where we also present the periods of the time crystalline phase obtained through Monte Carlo simulations [61].

To summarize, we compare semiclassical and quantum approaches: In Fig. 2 we observe the appearance of limit

cycles for driving amplitudes between the points H_1 and H_2 which indicates a broken continuous time translation symmetry of the set of equations (3) within this interval of $\mathcal{E}_1$. This is manifested by the discrete peak structure in Figs. 2(d) and 2(e). In the quantum case we observe nearly nondecaying (almost zero real part of the Liouville eigenvalues) oscillating coherences at corresponding frequencies, see Figs. 3(c) and 3(d). Semiclassical peaks in Figs. 2(d) and 2(e) correspond to the points enclosed by the arrows and ovals in Figs. 3(c) and 3(d), respectively.

Conclusion.—In this Letter we demonstrated that a system of two coupled bosonic modes in a dissipative cavity exhibits rich behavior related to time crystalline phases. Based on the semiclassical approach, we have identified a wide parameter range in which a time crystalline phase emerges in the form of usual limit cycles as well as a new kind of novel unexpected limit cycle featuring a doubled-loop structure associated with period doubling. The use of the powerful bifurcation theory turned out to be essential in uncovering the rich dynamical scenarios of our system. Results of computations in the quantum regime in the identified parameter range qualitatively agree with the global picture sketched by the semiclassical approach: A series of quantum phase transitions is observed with oscillating coherences at a range of parameters where, semiclassically, Hopf and period-doubling bifurcations emerge. These quantum transitions are accompanied by the closure of the Liouvillian gap in the thermodynamic limit. Computational limitations do not allow us to probe the system at sufficiently large excitation number N to make more precise, quantitative predictions on the phase transitions of the model discussed in this Letter. At this stage, experimental investigations, like in [7,8,10,11] are the natural next step for a detailed investigation of the predicted nonequilibrium phase transitions.

We would like to express our gratitude to the group of Dr. Philippe Corboz at the University of Amsterdam for allowing us to use their high capacity workstations to perform long-running computations on the quantum trajectories. L. R. B., M. S. B., D. V. K., and A. K. F. are thankful for the support by the Russian Science Foundation Grant No. 20-42-05002 (exact algebraic solution and semiclassical analysis) and the Russian Roadmap on Quantum Computing (exact diagonalization calculations). M. S. B. thanks Basic Research Program of HSE for the provided support. The work by V. G. is part of the DeltaITP consortium, a program of the Netherlands Organization for Scientific Research (NWO) funded by the Dutch Ministry of Education, Culture and Science (OCW). Finally, some computations have been carried out using computational resources of the HPC cluster at the HSE University, Moscow, Russia.

*Corresponding author.
l.bakker@friam.nl

[1] N. Imoto, H. A. Haus, and Y. Yamamoto, Phys. Rev. A **32**, 2287 (1985).
[2] S. E. Harris, J. E. Field, and A. Imamoğlu, Phys. Rev. Lett. **64**, 1107 (1990).
[3] Q. A. Turchette, C. J. Hood, W. Lange, H. Mabuchi, and H. J. Kimble, Phys. Rev. Lett. **75**, 4710 (1995).
[4] S. Kumar and D. P. DiVincenzo, Phys. Rev. B **82**, 014512 (2010).
[5] D. E. Chang, V. Vuletić, and M. D. Lukin, Nat. Photonics **8**, 685 (2014).
[6] D. England, F. Bouchard, K. Fenwick, K. Bonsma-Fisher, Y. Zhang, P. J. Bustard, and B. J. Sussman, Appl. Phys. Lett. **119**, 160501 (2021).
[7] M. Zhang, C. Wang, Y. Hu, A. Shams-Ansari, T. Ren, S. Fan, and M. Lončar, Nat. Photonics **13**, 36 (2019).
[8] X. Xue, X. Zheng, and B. Zhou, Nat. Photonics **13**, 616 (2019).
[9] X. Xu, M. Tan, J. Wu, R. Morandotti, A. Mitchell, and D. J. Moss, IEEE Photonics Technol. Lett. **31**, 1854 (2019).
[10] A. Tikan, J. Riemensberger, K. Komagata, S. Hnl, M. Churaev, C. Skehan, H. Guo, R. N. Wang, J. Liu, P. Seidler, and T. J. Kippenberg, Nat. Phys. **17**, 604 (2021).
[11] N. Englebert, F. D. Lucia, P. Parra-Rivas, C. M. Arabí, P.-J. Sazio, S.-P. Gorza, and F. Leo, Nat. Photonics **15**, 857 (2021).
[12] D. Gottesman, A. Kitaev, and J. Preskill, Phys. Rev. A **64**, 012310 (2001).
[13] A. Grimm, N. E. Frattini, S. Puri, S. O. Mundhada, S. Touzard, M. Mirrahimi, S. M. Girvin, S. Shankar, and M. H. Devoret, Nature (London) **584**, 205 (2020).
[14] B. Yurke and D. Stoler, Phys. Rev. Lett. **57**, 13 (1986).
[15] G. Kirchmair, B. Vlastakis, Z. Leghtas, S. E. Nigg, H. Paik, E. Ginossar, M. Mirrahimi, L. Frunzio, S. M. Girvin, and R. J. Schoelkopf, Nature (London) **495**, 205 (2013).
[16] H. Alaeian, G. Giedke, I. Carusotto, R. Löw, and T. Pfau, Phys. Rev. A **103**, 013712 (2021).
[17] H. Alaeian, M. Soriente, K. Najafi, and S. F. Yelin, arXiv:2106.04045.
[18] C. Lledó, T. K. Mavrogordatos, and M. H. Szymańska, Phys. Rev. B **100**, 054303 (2019).
[19] W. Casteels, R. Fazio, and C. Ciuti, Phys. Rev. A **95**, 012128 (2017).
[20] K. Seibold, R. Rota, and V. Savona, Phys. Rev. A **101**, 033839 (2020).
[21] J. A. Muniz, D. Barberena, R. J. Lewis-Swan, D. J. Young, J. R. K. Cline, A. M. Rey, and J. K. Thompson, Nature (London) **580**, 602 (2020).
[22] C. Lledó and M. H. Szymańska, New J. Phys. **22**, 075002 (2020).
[23] D. Roberts and A. A. Clerk, Phys. Rev. X **10**, 021022 (2020).
[24] Z. Gong, R. Hamazaki, and M. Ueda, Phys. Rev. Lett. **120**, 040404 (2018).
[25] M. Ippoliti, K. Kechedzhi, R. Moessner, S. L. Sondhi, and V. Khemani, PRX Quantum **2**, 030346 (2021).
[26] J. G. Cosme, J. Skulte, and L. Mathey, Phys. Rev. A **100**, 053615 (2019).
[27] H. Keßler, J. G. Cosme, C. Georges, L. Mathey, and A. Hemmerich, New J. Phys. **22**, 085002 (2020).
[28] H. Alaeian and B. Buča, arXiv:2202.09369.

[29] B. Buča and D. Jaksch, Phys. Rev. Lett. **123**, 260401 (2019).
[30] B. Buča, J. Tindall, and D. Jaksch, Nat. Commun. **10** (2019).
[31] S. P. Kelly, E. Timmermans, J. Marino, and S.-W. Tsai, SciPost Phys. Core **4**, 21 (2021).
[32] N. Y. Yao and C. Nayak, Phys. Today **71**, No. 9, 40 (2018).
[33] J. Zhang, P. W. Hess, A. Kyprianidis, P. Becker, A. Lee, J. Smith, G. Pagano, I.-D. Potirniche, A. C. Potter, A. Vishwanath, N. Y. Yao, and C. Monroe, Nature (London) **543**, 217 (2017).
[34] S. Choi, J. Choi, R. Landig, G. Kucsko, H. Zhou, J. Isoya, F. Jelezko, S. Onoda, H. Sumiya, V. Khemani, C. von Keyserlingk, N. Y. Yao, E. Demler, and M. D. Lukin, Nature (London) **543**, 221 (2017).
[35] X. Mi and M. I. *et al.*, Nature (London) **601**, 531 (2022).
[36] H. Keßler, P. Kongkhambut, C. Georges, L. Mathey, J. G. Cosme, and A. Hemmerich, Phys. Rev. Lett. **127**, 043602 (2021).
[37] N. Dogra, M. Landini, K. Kroeger, L. Hruby, T. Donner, and T. Esslinger, Science **366**, 1496 (2019).
[38] F. Wilczek, Phys. Rev. Lett. **109**, 160401 (2012).
[39] V. Khemani, R. Moessner, and S. L. Sondhi, arXiv:1910.10745.
[40] K. Sacha and J. Zakrzewski, Rep. Prog. Phys. **81**, 016401 (2018).
[41] D. V. Else, C. Monroe, C. Nayak, and N. Y. Yao, Annu. Rev. Condens. Matter Phys. **11**, 467 (2020).
[42] P. Glendinning, *Stability, Instability and Chaos: An Introduction to the Theory of Nonlinear Differential Equations*, Cambridge Texts in Applied Mathematics (Cambridge University Press, Cambridge, England, 1994).
[43] P. D. Drummond and D. F. Walls, J. Phys. A **13**, 725 (1980).
[44] N. Bartolo, F. Minganti, W. Casteels, and C. Ciuti, Phys. Rev. A **94**, 033841 (2016).
[45] V. Gritsev and A. Polkovnikov, SciPost Phys. **2**, 021 (2017).
[46] M. Ringel and V. Gritsev, Phys. Rev. A **88**, 062105 (2013).
[47] L. R. Bakker, V. I. Yashin, D. V. Kurlov, A. K. Fedorov, and V. Gritsev, Phys. Rev. A **102**, 052220 (2020).
[48] S. Charzyński and M. Kuś, J. Phys. A **46**, 265208 (2013).
[49] J. Wei and E. Norman, J. Math. Phys. (N.Y.) **4**, 575 (1963).
[50] J. Wei and E. Norman, Proc. Am. Math. Soc. **15**, 327 (1964).
[51] M. O. Scully and M. S. Zubairy, *Quantum Optics* (Cambridge University Press, Cambridge, England, 1997).
[52] See Supplemental Material at http://link.aps.org/supplemental/10.1103/PhysRevLett.129.250401 for more detailed information. The Supplemental Material includes Ref. [53].
[53] F. Pietracaprina, N. Mac, D. J. Luitz, and F. Alet, SciPost Phys. **5**, 45 (2018).
[54] *Quantum Optics*, edited by D. Walls and G. J. Milburn (Springer, Berlin Heidelberg, 2008).
[55] The presence of two-photon losses is not essential and can be omitted, at least at the semiclassical level. For completeness we keep it under consideration in this Letter.
[56] G. Lindblad, Commun. Math. Phys. **48**, 119 (1976).
[57] D. O. Krimer and M. Pletyukhov, Phys. Rev. Lett. **123**, 110604 (2019).
[58] J. Guckenheimer and P. Holmes, *Nonlinear Oscillations, Dynamical Systems, and Bifurcations of Vector Fields* (Springer, New York, 1983).
[59] A. Dhooge, W. Govaerts, Y. A. Kuznetsov, H. G. Meijer, and B. Sautois, Math. Comp. Model. Dyn. Sys. **14**, 147 (2008).
[60] H. J. Carmichael, Phys. Rev. X **5**, 031028 (2015).
[61] J. Johansson, P. Nation, and F. Nori, Comput. Phys. Commun. **184**, 1234 (2013).